Thermochimica Acta 742 (2024) 179894

Contents lists available at ScienceDirect

Thermochimica Acta

journal homepage: www.elsevier.com/locate/tca

Characterization of thermal behavior of two types of kaolin in China by ultrafast Joule heating combined with XRD, FT-IR, TG-DSC and SEM

Jiahang Fan, Xianjie Liu, Mingyong Liu, Mengyao Yang, Yuena Jiang, Ruiyu Mi, Xin Min, Zhaohui Huang *

Engineering Research Center of Ministry of Education for Geological Carbon Storage and Low Carbon Utilization of Resources, Beijing Key Laboratory of Materials Utilization of Nonmetallic Minerals and Solid Wastes, National Laboratory of Mineral Materials, School of Materials Science and Technology, China University of Geosciences Beijing, 100083, China

ARTICLE INFO

Keywords:
Kaolin
Ultrafast Joule heating
Thermal behavior analysis
Mineral phase transition
Mullite

ABSTRACT

Thermal behavior of sandy kaolin selected from Guangxi and hard kaolin from Inner Mongolia in China were characterised by ultrafast Joule heating combined with XRD, FT-IR, TG-DSC and SEM. The results indicated that the sandy kaolin was composed of kaolinite, muscovite and quartz, and hard kaolin was predominantly composed of kaolinite, with minor quantities of anatase. During ultrafast Joule heating, the layered structure of kaolinite of sand kaolin was destroyed, and all hydroxyl groups were lost at 700 °C, while dehydroxylation completion of the hard kaolin at higher temperature, accompanied by rupture of lamellar kaolinite. Muscovite disappeared completely and accompanied by the formation of mullite at 1100 °C, while quartz is relatively unaffected, resulting in the sandy kaolin consisting of quartz and mullite phases at 1200 °C. In contrast, the transformation rate and crystallinity of mullite phase of hard kaolin was significantly higher than that of sandy kaolin.

1. Introduction

Kaolin is an important clay mineral that is used in paper, ceramics, refractories, rubber, water pollution treatment, zeolite preparation and other applications because of its good properties [1–4]. China has been using kaolin as a raw material for firing fine porcelain since the Tang Dynasty, such as the famous "Tang sancai ceramics", which is made of kaolin as a tyre and fired with yellow, green and blue glazes [5]. According to the quality, plasticity and sand content, kaolin in China can be divided into three types of hard kaolin, soft kaolin and sandy kaolin, both hard kaolin and soft kaolin belong to coal series kaolin [6]. The mineral composition of kaolin is related to its ore-forming parent rock and mineralising environment [7,8], includes kaolin group clay minerals, e.g. kaolinite, halloysite, dickite and nacrite, and other associated impurity minerals, such as feldspar, quartz, mica, pyrite and rutile, etc. [9,10]. Kaolinite ($Al_2O_3{\cdot}2SiO_2{\cdot}2H_2O$) is a 1:1 layered aluminosilicate clay mineral, which consisting of a silica-oxygen tetrahedral layer $[SiO_4]^{4-}$ and an aluminium-oxygen octahedral layer $\{Al[O_2(OH)_4]\}^{6-}$ connected along the two-dimensional direction to form the structural unit layer of kaolinite, e.g. $\{Al_4[Si_4O_{10}(OH)_8]\}$, the layers are connected to other layers via hydrogen bonds, and the layer spacing is about 7.2 Å [11].

The thermal evolution of kaolin in the temperature range of 400 to 1200 °C has been a controversial issue [12], and a great deal of work has been carried out by researchers to study the thermal behaviour of kaolin [13–16]. It is certain that the thermal treatment causes atomic rearrangement of kaolin, and the process is accompanied by dehydroxylation of kaolinite or the formation of intermediate crystalline phase and new phase [17–20]. In general, the heating equipment used to study the thermal behaviour of kaolin is a muffle furnace [21]. However, the heat generated by the muffle furnace during heating and cooling inevitably affects the structure of the kaolin, on the other hand, due to the long holding time (2–6 h), the results of current research often do not agree with TG-DSC [13]. In order to accurately evaluate the thermal behaviour of kaolin and make it consistent with the results of TG-DSC, kaolin was heated by ultrafast Joule heating technique in this work. ultrafast Joule heating with ultrafast heating rate (~10^5 °C/s) and cooling rate (~10^4 °C/s) [22,23], which avoids the effects of residual heat generated by muffle furnace. In addition, ultrafast Joule heating can be custom programmed to control temperature with excellent

* Corresponding author.
E-mail address: huang118@cugb.edu.cn (Z. Huang).

https://doi.org/10.1016/j.tca.2024.179894
Received 31 August 2024; Received in revised form 20 October 2024; Accepted 1 November 2024
Available online 2 November 2024

controllability and accuracy [24], which can provide new research support for the thermal behaviour of kaolin in combination with other characterisation methods.

This work presents the thermal behaviour analysis of two types of kaolin subjected to ultrafast Joule heating from 400 to 1200 °C, selected from different regions in China. The experimental results demonstrated that ultrafast Joule heating in conjunction with other characterisation techniques offers a reliable approach for investigating the physical phase and structural transformation of kaolin during the heating process. Furthermore, this method may serve as a reference for studying the thermal behaviour of other minerals or materials.

2. Experimental

2.1. Materials

Two kaolin raw materials used in this study were sourced from Guangxi Zhuang Autonomous Region, China (sandy kaolin, SKaol) and Inner Mongolia Autonomous Region, China (hard kaolin, HKaol). The two raw kaolin samples were ground to 200 meshs and sieved to a particle size of below 74 μm, then dried at 110 °C for 24 h. The chemical compositions of kaolin samples are shown in Table 1, indicating that the content of major components such as SiO_2 and K_2O is higher in SKaol than in HKaol, while the content of Al_2O_3 is lower in SKaol, which suggests the possibility that SKaol may contain a greater proportion of quartz and muscovite minerals, a hypothesis that requires further verification through XRD analysis. However, the content of other impurities, including Fe_2O_3, TiO_2 and CaO is higher in HKaol than in SKaol, with TiO_2 exhibiting the greatest discrepancy. The 200 mg of kaolin sample was heated at 400, 500, 600, 700, 800, 900, 1000, 1100 and 1200 °C for 1 min in a ultrafast Joule heating furnace under an air atmosphere, respectively. The schematic diagram of ultrafast Joule heating and the heating curve at 1000 °C (similar heating curves for other temperatures) are presented in Fig. 1.

2.2. Characterization

X-ray diffractometer (XRD, Bluker D8 Advance, Germany) was used to analyze the mineral composition of the raw and the flash heating treated kaolin samples. The conditions for the determination were as follows: The CuKα radiation source was operated in normal scanning mode (λ = 0.154 nm) at 40 kV and 40 mA, with a scanning rate of 5 °/min in the range of 5°−70° (2θ).

Fourier transform infrared spectroscopy (FT-IR, Thermo Scientific Nicolet iS20, USA) was employed to obtain FTIR spectra of kaolin samples within the wave number range of 400–4000 cm^{-1}. The kaolin samples were finely ground in a ceramic mortar and thoroughly mixed with potassium bromide (KBr) pellets (ca. 2 % by mass in KBr).

Thermogravimetry and differential scanning analysis (TG-DSC, PerkinElmer STA 8000, USA) were employed to ascertain the thermal stability and reaction heat of two distinct types of kaolin samples. About 20 mg of samples underwent thermal analysis with a heating rate of 10 °C/min from 30 °C to 1200 °C in air atmosphere (O_2/N_2≈1:4).

Scanning electron microscope (SEM, ZEISS SUPRA55, Germany) was employed to observe the morphology of the raw and the heated kaolin samples. The kaolin samples were dispersed on a conductive adhesive, affixed to a circular aluminium electron microscope plate, and the samples were metallised with gold to ensure conductivity prior to observation.

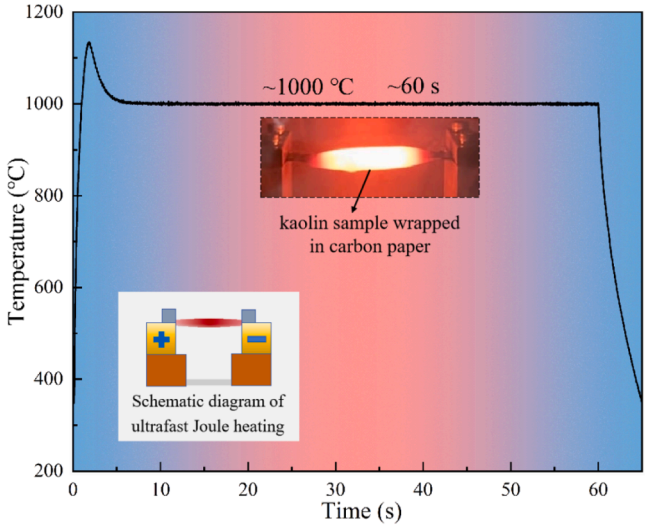

Fig. 1. Schematic diagram of ultrafast Joule heating and curve of kaolin sample heated at 1000 °C for 1 min.

3. Results and discussion

3.1. XRD analysis

The XRD patterns of the two raw kaolin samples are shown in Fig. 2. The main mineralogical compositions of Skao sample were determined

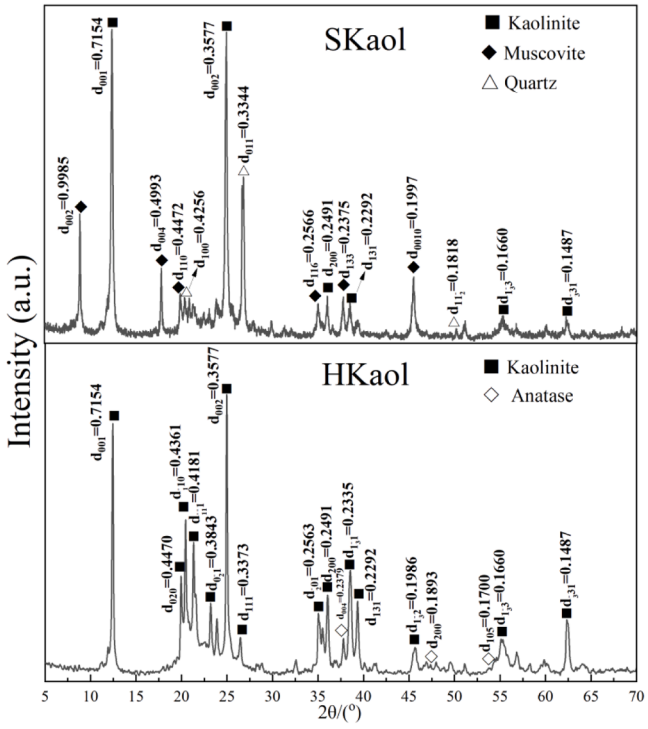

Fig. 2. XRD patterns of sandy kaolin and hard kaolin.

Table 1
Chemical composition of the two raw kaolin samples (wt%).

	SiO_2	Al_2O_3	K_2O	Fe_2O_3	TiO_2	P_2O_5	MgO	ZrO_2	CaO	SO_3	Others
SKaol	54.96	40.64	2.59	1.13	0.14	0.17	0.17	—	—	—	0.22
HKaol	47.60	47.00	0.27	1.27	2.33	0.21	0.12	0.09	0.86	0.15	0.10

as kaolinite (PDF card NO 79–1570), muscovite (PDF card NO 80–0742) and quartz (PDF card NO 85–0797), and the semi-quantitative analytical compositions of the three minerals are 68.7 %, 24.2 %, and 7.1 %, respectively. The main characteristic diffraction peaks of kaolinite were observed at approximately 2θ =12.407°, 24.962° and 55.39°, with corresponding *d* values of 0.7154, 0.3577 and 0.1660 nm. The main diffraction peaks of muscovite were observed at 2θ =8.85°, 17.754° and 45.386°, with corresponding *d* values of 0.9985, 0.4993 and 0.1997 nm. The main peaks of quartz were observed at 2θ = 20.856°, 26.639°, 50.139° and exhibited *d* values of 0.4256, 0.3344 and 0.1818 nm, respectively. The presence of muscovite and quartz has been observed to increase the K_2O and SiO_2 content of the Skaol, which is consistent with the results of the XRF analyses. The diffraction peaks of the HKaol were highly matched with kaolinite (PDF card NO 79–1570), and the characteristic peaks and corresponding *d* values of the kaolinite of HKaol are in agreement with the above. In addition, weak anatase diffraction peaks (PDF card NO 99–0008) were found in HKaol, with the main characteristic peaks were observed at 2θ =37.792°, 48.035° and 53.884° and exhibited *d* values of 0.2379, 0.1893 and 0.1700 nm, respectively. and the information of other characteristic peaks are shown in Fig. 2.

The XRD patterns of both kaolin samples subjected to ultrafast Joule heating at 400–1200 °C for 1 min are shown in Fig. 3 and 4. As illustrated in Fig. 3, the intensity of all diffraction peaks of kaolinite (12.407°, 24.962°, 36.091°, 39.4° and 55.39°) gradually weakened as the temperature increases, which disappeared completely when the temperature heated up to 700 °C. The results indicated that the loss of the hydroxyl and the transformation of kaolinite into metakaolinite [25]. In contrast, the diffraction peak intensity of muscovite and quartz is less affected by temperature below 700 °C. As illustrated in Fig. 4, the peak observed at 2θ = 12.362° for the HKaol sample persists until the temperature is increased by 800 °C, the results indicated that HKaol with higher kaolinite content contains more abundant hydroxyl groups and the transformation of kaolinite to metakaolinite necessitates a greater input of energy [26]. The intensities of characteristic diffraction peaks for muscovite in the Skaol gradually decreased and disappeared completely when the temperature heated up to 700–1100 °C, and some new weak characteristic diffraction peaks were observed at 2θ = 16.4°, 26.171°, 33.149°, 35.196° and 42.535°, which were attributed to the emergence of mullite, and indicating that the pyrolysis energy of the muscovite is higher. However, the quartz diffraction peaks remained unchanged, indicating that the quartz structure is relatively inert and less susceptible to change when subjected to ultrafast Joule heating in this temperature range, the result is that Skaol consists of mullite and quartz at a temperature of 1200 °C. As illustrated in Fig. 4, all kaolinite

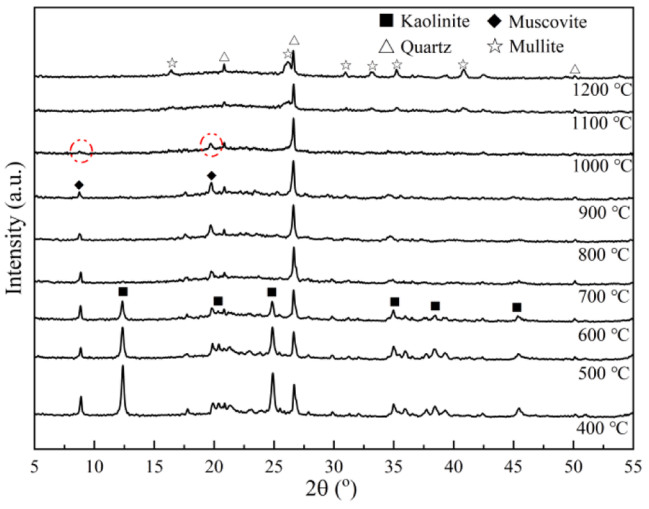

Fig. 3. XRD patterns of SKaol subjected to ultrafast Joule heating at 400 −1200 °C for 1 min.

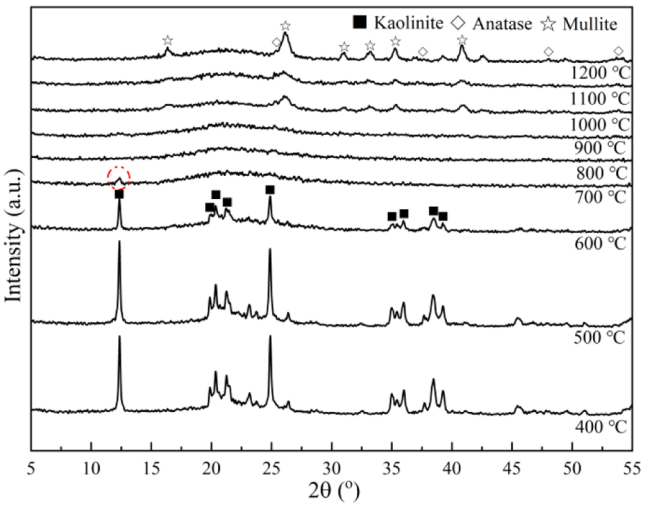

Fig. 4. XRD patterns of HKaol subjected to ultrafast Joule heating at 400 −1200 °C for 1 min.

diffraction peaks of HKaol disappeared completely when the temperature heated up to 800 °C, but some new weak diffraction peaks were observed at 2θ =16.4°, 26.171°, 35.196° and 40.804° when the temperature heated up to 1000 °C, and the intensity of these diffraction peaks gradually increased and sharpened when the temperature heated up to 1200 °C. Nevertheless, the transformation of anatase is not induced by ultrafast Joule heating, and it remains unaffected within the temperature range of 400–1200 °C. This results indicated that the kaolinite in HKaol has been completely transformed into an amorphous phase at 800 °C, then it transforms to the mullite phase at 1000 °C, and the degree of crystallinity in mullite increased with rising temperatures, in light of the abrupt ordering process of the premullite spinel structure, this phenomenon can be attributed to the migration of tetrahedral aluminium to octahedral positions, which ultimately leads to the formation of mullite [20], the final HKaol composition is comprised of mullite and anatase at 1200 °C. Similarly, this indicates that a greater energy input is necessary for the transformation of SKaol containing muscovite to mullite, which is in accordance with the findings of other researchers in this field [15].

3.2. FT-IR analysis

The infrared absorption spectra of raw kaolin samples is shown in Fig. 5. two bands were observed at 3695 and 3619 cm^{-1} for SKaol (HKaol was 3693 and 3620 cm^{-1}) in the high-wavenumber region (4000–3000 cm^{-1}), the 3695 or 3693 cm^{-1} was attributed to the symmetrical in-phase vibration of surface hydroxyl, and 3619 or 3620 cm^{-1} was associated with the stretching vibration modes of inner hydroxyl [26]. Three absorption peaks were observed at 1115, 1031 and 1007 cm^{-1} for SKaol (HKaol was 1099, 1034 and 1011 cm^{-1}) in the middle and low wavenumber region (1500–1000 cm^{-1}), these peaks were related to the symmetric stretching vibration of the Si-O-Si bond in the tetrahedral sheet [27]. In the low-wavenumber region (1000–400 cm^{-1}), several well-defined absorption bands were observed, the band at approximately 912 cm^{-1} for SKaol (HKaol was 914 cm^{-1}) was attributed to the Al-OH bending vibrational absorption peak, the 794, 754 and 695 cm^{-1} peaks for SKaol (HKaol was 789, 753 and 694 cm^{-1}) were attributed to the combination of Si-O-Al vibrations and the stretching vibration mode of inner hydroxyl [28], and the bands at 537, 469 and 429 cm^{-1} for SKaol (HKaol was 540, 471 and 432 cm^{-1}) were associated with the bending vibration mode of Si-O-Al [14].

The FT-IR spectra of both kaolin samples subjected to ultrafast Joule heating at 400–1200 °C for 1 min are presented in Fig. 6 and 7. As illustrated in Fig. 6, the intensity of the stretching vibration of the

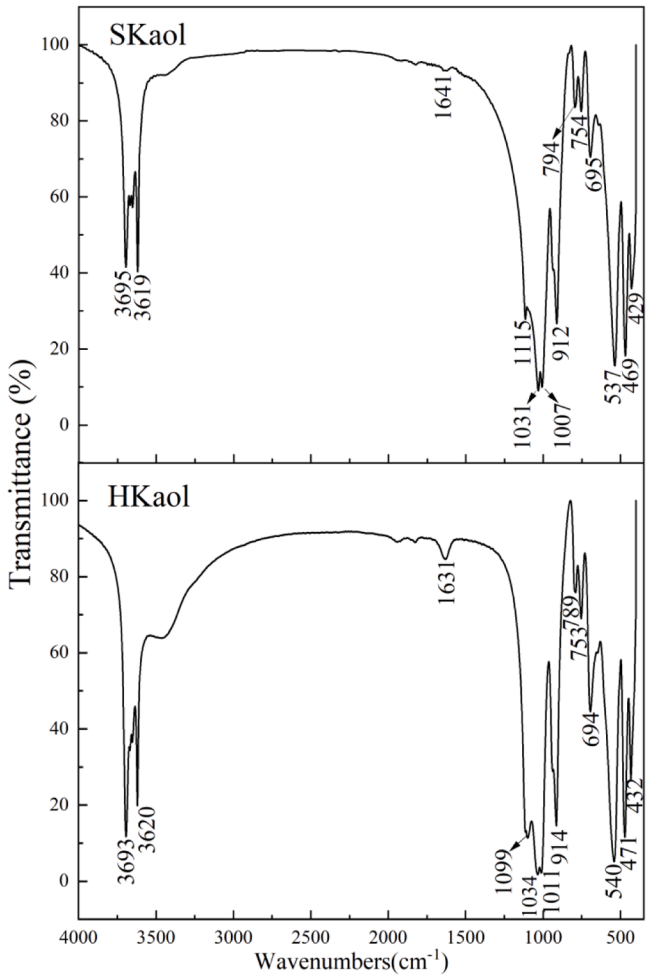

Fig. 5. FT-IR spectra of sandy kaolin and hard kaolin.

surface hydroxyl and the inner hydroxyl (3692 and 3619 cm^{-1}) for Skaol decreases significantly at 700 °C and disappeared completely when the temperature heated up to 1100 °C. Combined with the analysis of the XRD results, it can be suggested that kaolinite completed the dehydroxylation at 700 °C, while muscovite continued to dehydroxylate from 800 to 1100 °C. As illustrated in Fig. 7, the intensity of the two bands at 3693 and 3620 cm^{-1} for HKaol gradually decreases and disappeared at 800 °C, resulting in the complete dehydroxylation of kaolinite and the formation of amorphous metakaolinite, and the reaction equation is given below for reference [29].

$$2SiO_2{\cdot}Al_2O_3{\cdot}2H_2O\ (\text{Kaolinite}) \rightarrow 2SiO_2{\cdot}Al_2O_3\ (\text{Metakaolinite}) + 2H_2O\uparrow$$

The intensities of the bands at 1115, 1031 and 1002 cm^{-1} for SKaol (HKaol was 1115, 1031 and 1011 cm^{-1}) also gradually decreased as the temperature increases. The intensity of these peaks almost disappears at 800 °C for HKaol, while Skaol still has weakly intense peaks above 800 °C, which was attributed to the quartz structure is not damaged under these heating conditions. The intensities of the bands at 912, 794, 754, 695, 535 and 469 cm^{-1} for SKaol (HKaol was 914, 789, 753, 694, 534 and 471 cm^{-1}) gradually weakened and disappeared as the temperature increases, the result was attributed to the breakages of Al–OH, Si–O–Al as temperature increases for two kaolins [14], this is in agreement with the XRD analysis results.

3.3. TG-DTG-DSC analysis

The TG-DTG-DSC curves of raw kaolins are shown in Fig. 8 and Fig. 9. The advantage of ultrafast Joule heating is that it allows for precise control of the heating time at each temperature, from 400 to 1200 °C, to match the TG-DTG-DSC heating process. Furthermore, there is no heat interference caused by the heating and cooling during calcination, which ensures that the results of the TG-DTG-DSC can achieve a high degree of matching with the ultrafast Joule heating process. As illustrated in Fig. 8 and Fig. 9, as the raw kaolin samples were pre-dried, any moisture adsorbed on the surface is removed during this time, this results in a smooth TG curve until 200 °C and a low mass loss. A smaller reduction in the weight of kaolin is observed at temperature up to 400 °C, with the mass loss of 0.75 % and 1.39 % respectively, indicating the commencement of the dehydroxylation process of kaolin. The endothermic peaks were observed at 510.7 and 505.8 °C, with the mass loss of 10.25 % and 14.02 % in the temperature range of 400 to 700 °C, respectively, which was attributed to the structural hydroxyl desorption in the form of water from kaolinite. Consequently, the reaction underwent a transformation from $Al_2O_3{\cdot}2SiO_2{\cdot}2H_2O$ (kaolinite) to $Al_2O_3{\cdot}2SiO_2$ (metakaolinite) [30]. The total mass loss (15.41 %) of HKaol is significantly higher than that (11 %) of Skaol, and slightly higher than the theoretical loss rate of kaolinite structural water (14.4 %) [31]. The exothermic peaks were observed at 995.1 and 994.7 °C, with the mass loss of 0.82 % of Skaol was observed in the temperature range of 700 to 1100 °C, the phenomenon in question can be elucidated through the integration of XRD and FT-IR analyses, which reveal a correlation with the dehydroxylation of muscovite. While the dehydroxylation of HKaol was completed at 800 °C, and the mass remains stable or exhibits minor upward shifts after 800 °C, the upward shifts may be attributed to the instrumental factors. This exothermic phenomenon was ascribed to the transformation of metakaolinite into metastable Al-Si spinel and mullite [17], and the mullite was formed by the crystallisation function of amorphous products generated following the destruction of the kaolinite and muscovite in SKaol, this also explains why converting SKaol to mullite requires more energy input than HKaol. The outcomes yielded by TG-DSC are entirely consistent with those obtained by XRD and FT-IR analysis, thereby confirming the effectiveness of ultrafast Joule heating as a method for investigating the thermal behaviour of kaolin.

3.4. SEM analysis

The SEM patterns of the raw kaolin samples and the samples heated at 400, 700, 1000, 1200 °C are shown in Fig. 10-12. As illustrated in Fig. 10, the microstructure of kaolinite of SKaol and HKaol presented layered structure and sheet-like aggregate, respectively. As illustrated in Figs. 11 and 12, the morphology remains largely unaltered of kaolinite in two kaolins heated at 400 °C, and kaolinite loses all hydroxyl groups when the temperature rises to 700 °C, resulting in the collapse of the layered structure in SKaol and the crushing of the flake particles in HKaol. With the kaolin samples heated at 1000 °C, the layered structure of the kaolinite was completely destroyed and the appearance of adhesion between layers was observed in SKaol, while the particles appeared to melt, resulting in the formation of an amorphous phase in HKaol. Kaolinite melts significantly after heating at 1200 °C, accompanied by the formation of mullite from the amorphous phase, a phenomenon that is more pronounced in HKaol, which means that the transformation rate and crystallinity of mullite in HKaol is significantly higher than in Skaol, and the transformation of kaolin containing muscovite in SKaol into mullite requires a greater energy input, which is consistent with the previous analysis.

3.5. Analysis of the thermal evolution of kaolin

In summary, the schematic thermal evolution of two types of kaolin at ultrafast Joule heating for 1 min is shown in Fig. 13. At room temperature, the physical phase of the sandy kaolinite is characterised by the presence of layered kaolinite, muscovite and quartz. In contrast, the hard kaolinite is observed to form sheet-like kaolinite aggregates with

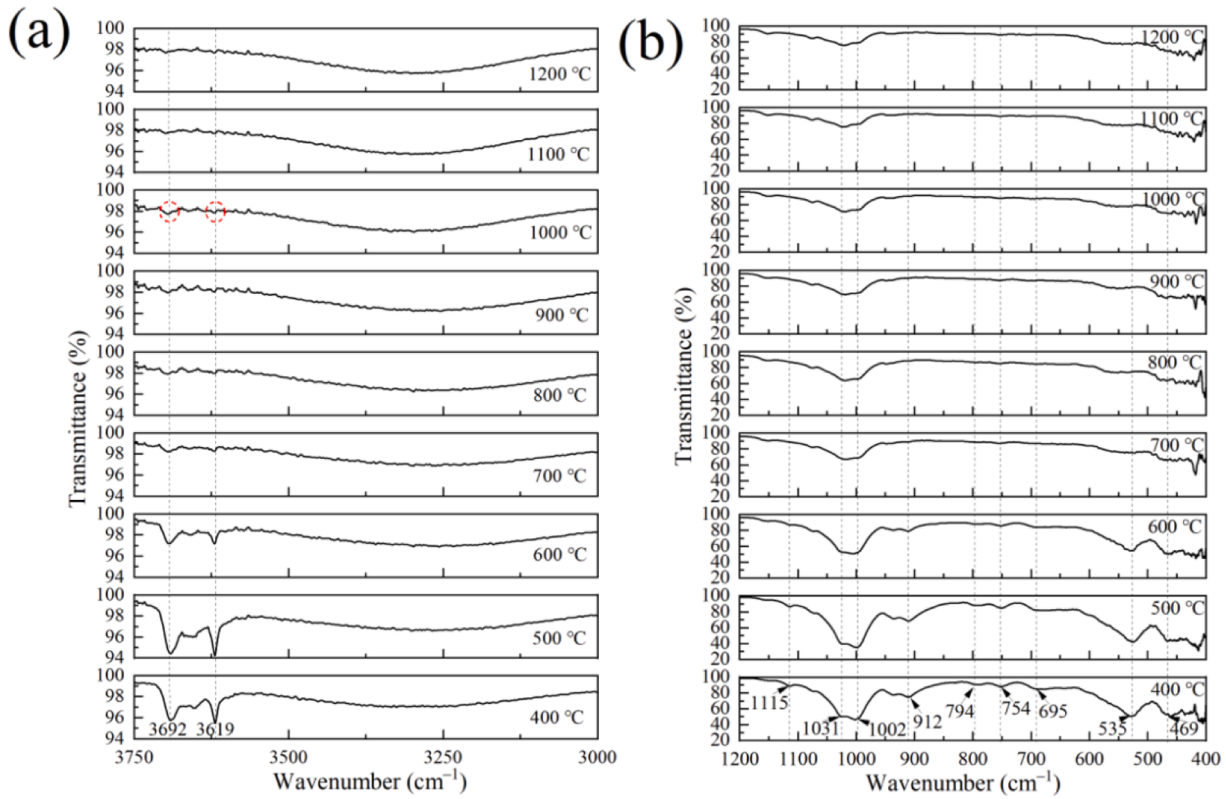

Fig. 6. FT-IR spectra of sandy kaolin heated at 400–1200 °C for 1 min: (a) 3000–3750 cm^{-1} and (b) 400–1200 cm^{-1}.

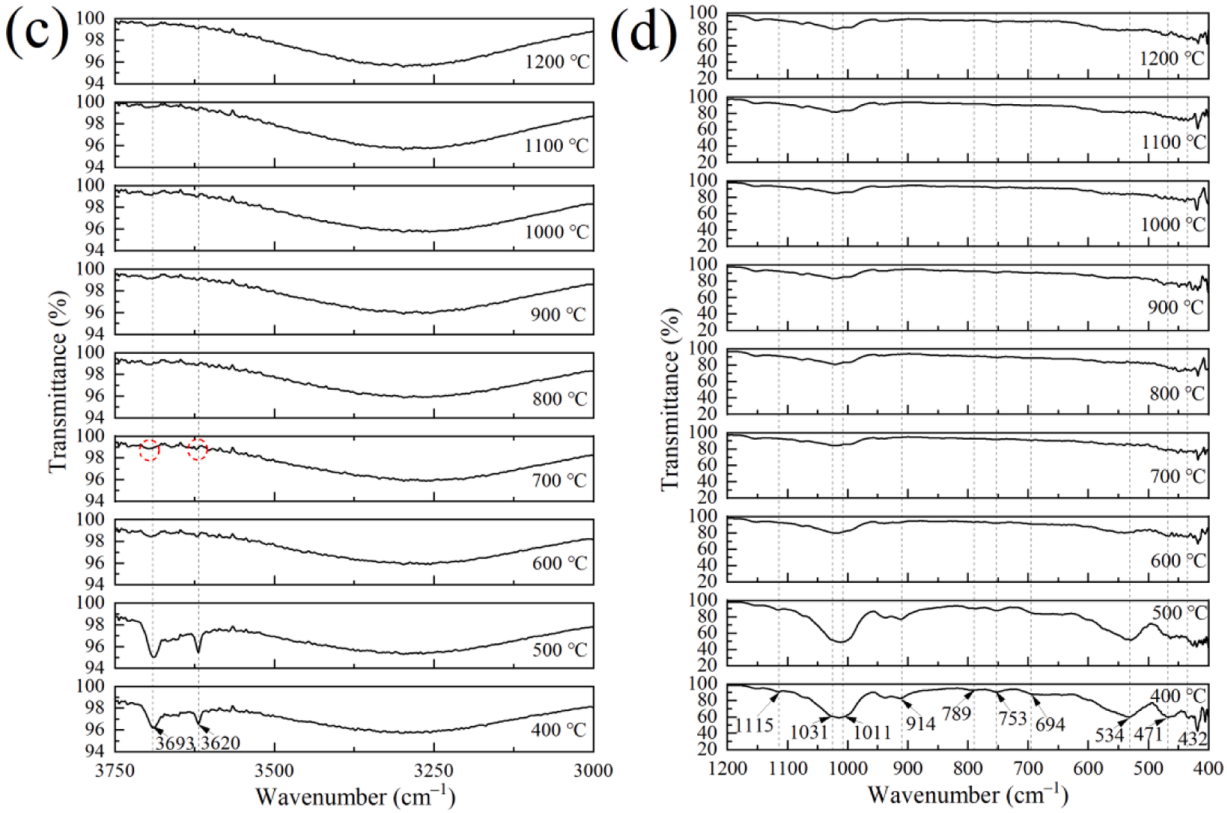

Fig. 7. FT-IR spectra of hard kaolin heated at 400–1200 °C for 1 min: (c) 3000–3750 cm^{-1} and (d) 400–1200 cm^{-1}.

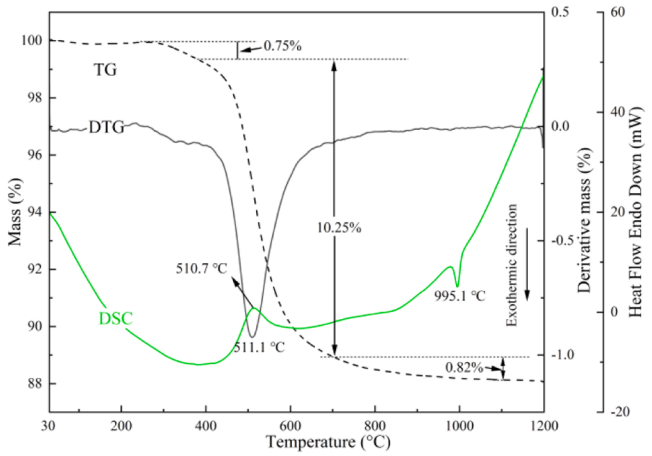

Fig. 8. TG-DTG-DSC curve of Skaol.

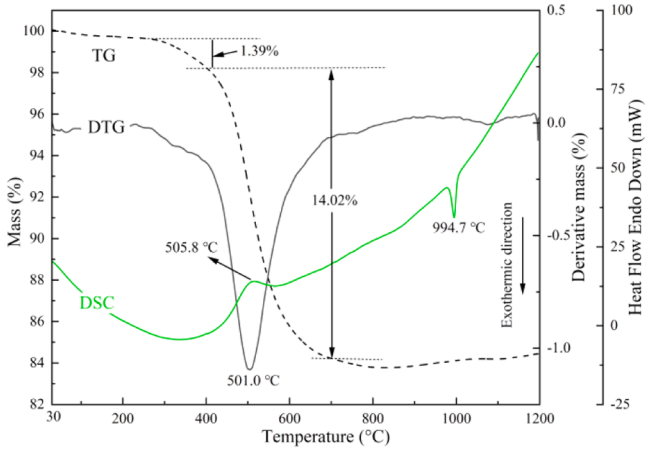

Fig. 9. TG-DTG-DSC curve of HKaol.

minor quantities of anatase. The kaolinite in Skaol completes dehydroxylation and is accompanied at 700 °C, whereas HKaol completely loses structural water at 800 °C due to its high kaolinite content, this dehydroxylation process leads to the break of Al-OH and Si-O-Al bonds, destroying the connection between the tetrahedral silica $[SiO_4]^{4-}$ sheet and octahedral alumina $\{Al[O_2(OH)_4]\}^{6-}$ sheet [32], the result is the collapse of layered kaolinite and the rupture of sheet-like kaolinite, this is also a necessary condition for the transformation of the physical phase. When the temperature rises to 1000 °C, the overwhelming majority of muscovite present in sandy kaolin loses its hydroxyl groups and assumes an amorphous structure. In contrast, the physical phase of hard kaolinite undergoes a shift towards mullite, which involved a transition from an amorphous, disordered state to a crystalline, ordered phase. At 1200 °C, the structure of muscovite in sandy kaolin is completely destroyed, and the amorphous phase formed by muscovite and kaolinite is transformed to mullite, while the Si-O-Si structure of quartz is not destroyed, and ultimately consists of two phases of mullite and quartz, while the transformation of kaolinite to mullite in hard kaolin is more complete, and the content and crystallinity of mullite increases.

4. Conclusion

This study introduces a novel heating method (ultrafast Joule heating) and combines it with XRD, FT-IR, TG-DTG and SEM to analyse the thermal behaviour of sandy kaolin (SKaol) and hard kaolin (HKaol) in China from 400 to 1200 °C. The results indicated that the mainly physical phase composition of Skaol consists of kaolinite, muscovite and quartz, whereas that of HKaol was predominantly composed of kaolinite, with minor quantities of anatase. The kaolinite in Skaol completes dehydroxylation and is accompanied by the collapse of the layered kaolinite structure at 700 °C, whereas HKaol completely loses structural water at 800 °C due to its high kaolinite content. Upon completion of dehydroxylation, HKaol undergoes a transformation into amorphous metakaolin, while the muscovite in Skaol is observed to disappear at 1100 °C, and the quartz phase is observed to be less affected by ultrafast Joule heating due to its inert chemical properties. The appearance of the mullite phase in HKaol was observed following heating at 1000 °C, which involved a transition from an amorphous, disordered state to a crystalline, ordered phase. The conversion of Skaol to mullite was observed to occur at 1100 °C, indicating that the energy required for this transformation is significantly higher than that of HKaol. Moreover, the conversion rate and crystallinity of mullite at 1200 °C of HKaol were found to be markedly higher than those of Skaol. The combination of ultrafast Joule heating with other characterisation methods allows for a highly precise account of the dynamic transformation of the physical phases and structure of kaolinite throughout the heating process, circumventing the influence of residual heat generated in the muffle furnace during the heating and cooling process on the structure of the kaolin, and also serves as a reference for the investigation of the thermal behaviour of other minerals or materials.

Author statement

In the following are reported the roles of each author involved in the submitted work “Characterization of thermal behavior of two types of kaolin in China by ultrafast Joule heating combined with XRD, FT-IR,

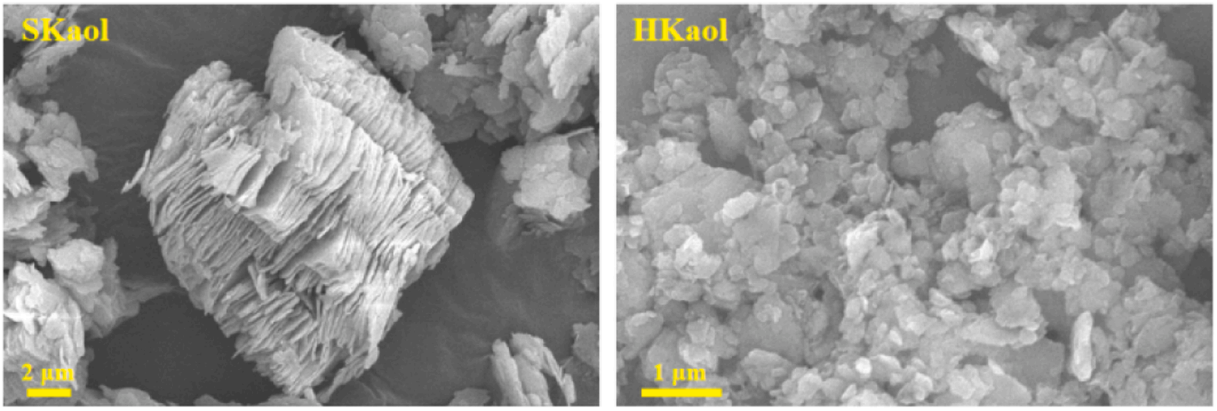

Fig. 10. SEM images of sand kaolin and hard kaolin.

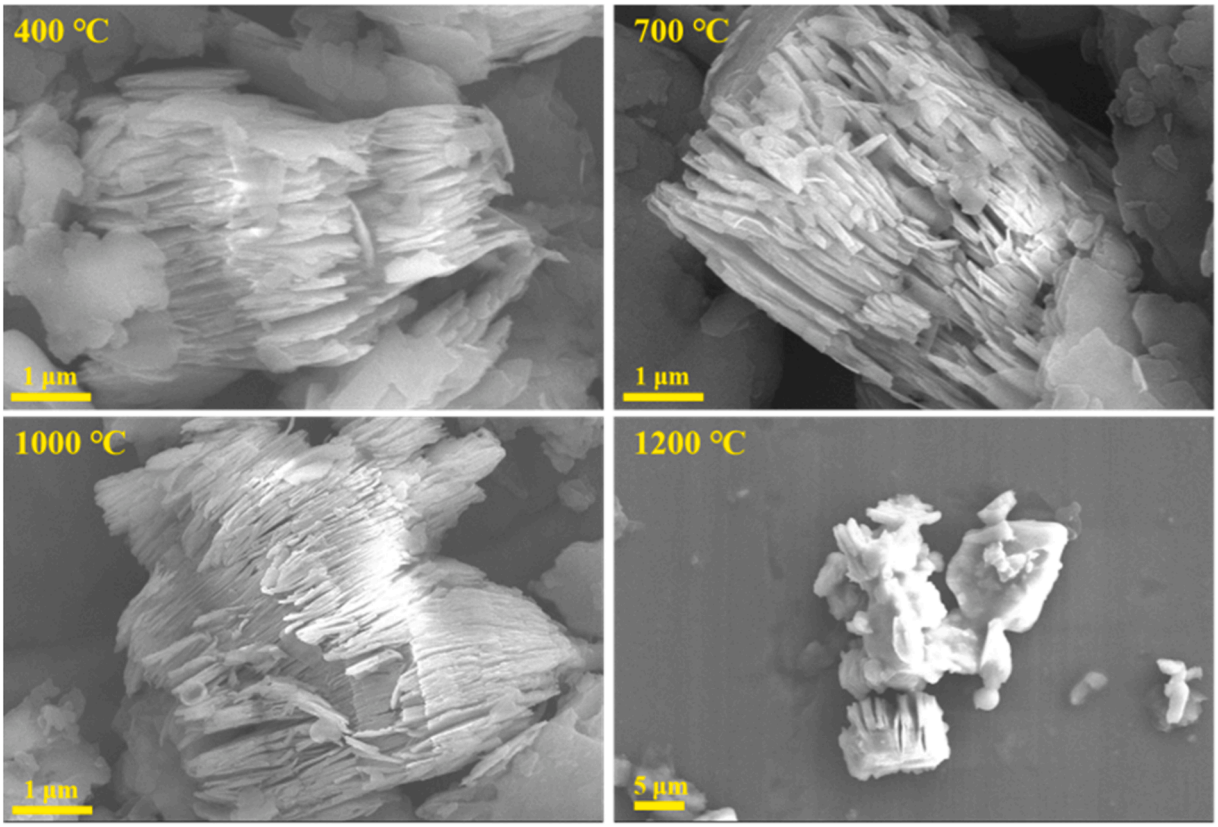

Fig. 11. SEM images of sandy kaolin heated at 400, 700, 1000 and 1200 °C for 1 min.

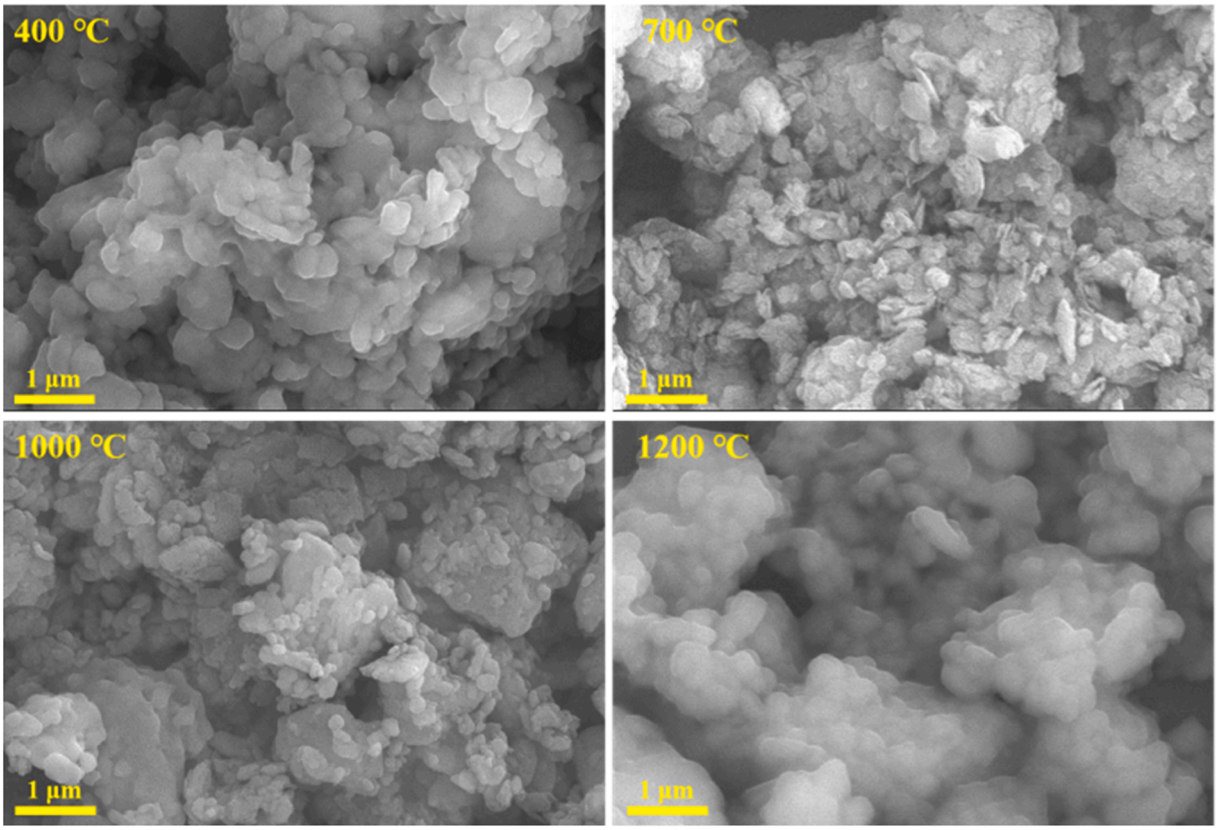

Fig. 12. SEM images of HKaol heated at 400, 700, 1000 and 1200 °C for 1 min.

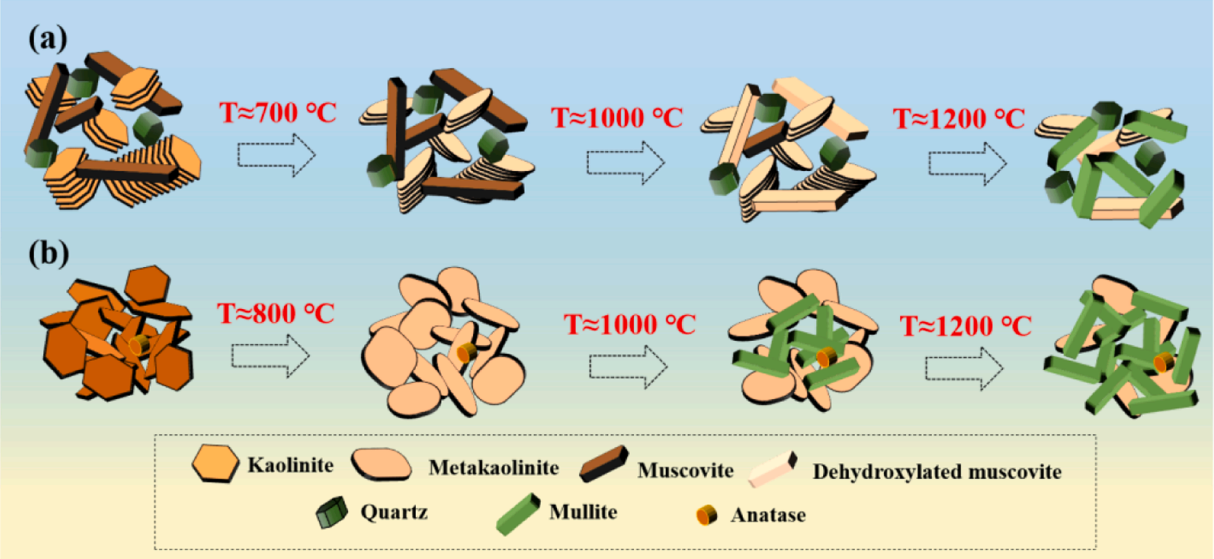

Fig. 13. Schematic thermal evolution of two types of kaolin by ultrafast Joule heating at different temperatures: (a) sandy kaolin; (b) hard kaolin.

TG-DSC and SEM" by Jiahang Fan, Xianjie Liu, Mingyong Liu, Mengyao Yang, Yuena Jiang, Ruiyu Mi, Xin Min and Zhaohui Huang to be published in the "*Thermochimica Acta*" Journal.

CRediT authorship contribution statement

Jiahang Fan: Writing – original draft, Visualization, Methodology, Formal analysis, Data curation, Conceptualization. **Xianjie Liu:** Writing – original draft, Visualization, Validation. **Mingyong Liu:** Validation, Methodology, Formal analysis. **Mengyao Yang:** Writing – original draft, Validation. **Yuena Jiang:** Validation, Formal analysis. **Ruiyu Mi:** Writing – review & editing, Visualization. **Xin Min:** Writing – review & editing, Visualization, Validation. **Zhaohui Huang:** Writing – review & editing, Visualization, Validation, Methodology.

Declaration of competing interest

The authors declared that they have no conflicts of interest to this work. We declare that we do not have any commercial or associative interest that represents a conflict of interest in connection with the work submitted.

Acknowledgements

This work was supported by the National Key R&D Program of China (2022YFC2904802)

Data availability

No data was used for the research described in the article.

References

[1] H.H. Murray, Traditional and new applications for kaolin, smectite, and palygorskite: a general overview, Appl. Clay. Sci. 17 (2000) 207–221, https://doi.org/10.1016/S0169-1317(00)00016-8.
[2] X. Qiu, X. Lei, A. Alshameri, H. Wang, C. Yan, Comparison of the physicochemical properties and mineralogy of Chinese (Beihai) and Brazilian kaolin, Ceram. Int. 40 (2014) 5397–5405, https://doi.org/10.1016/j.ceramint.2013.10.121.
[3] D.M. Liu, C. Dong, B. Xu, Preparation of magnetic kaolin embedded chitosan beads for efficient removal of hexavalent chromium from aqueous solution, J. Environ. Chem. Eng. 9 (2021) 105438, https://doi.org/10.1016/j.jece.2021.105438.
[4] S.M. Holmes, S.H. Khoo, A.S. Kovo, The direct conversion of impure natural kaolin into pure zeolite catalysts, Green. Chem. 13 (2011) 1152–1154, https://doi.org/10.1039/C1GC15099E.
[5] P.A. PSchroeder, G. Erickson, Kaolin: from ancient porcelains to nanocomposites, Elements 10 (2014) 177–182, https://doi.org/10.2113/gselements.10.3.177.
[6] N.J. Saikia, D.J. Bharali, P. Sengupta, D. Bordoloi, R.L. Goswamee, P.C. Saikia, P. C. Borthakur, Characterization, beneficiation and utilization of a kaolinite clay from Assam, India. Appl Clay Sci. 24 (2003) 93–103, https://doi.org/10.1016/S0169-1317(03)00151-0.
[7] G.I.E. Ekosse, Kaolin deposits and occurrences in Africa: geology, mineralogy and utilization, Appl Clay Sci. 50 (2010) 212–236, https://doi.org/10.1016/j.clay.2010.08.003.
[8] V.J. Hurst, S.M. Pickering, Origin and classification of coastal plain kaolins, southeastern USA, and the role of groundwater and microbial action, Clays. Clay. Miner. 45 (1997) 274–285, https://doi.org/10.1346/CCMN.1997.0450215.
[9] B. Biswas, M.R. Islam, A.K. Deb, A. Greenaway, L.N. Warr, R. Naidu, Understanding iron impurities in Australian kaolin and their effect on acid and heat activation processes of clay, ACS. Omega 8 (6) (2023) 5533–5544, https://doi.org/10.1021/acsomega.2c06795.
[10] H.G. Dill, Kaolin: soil, rock and ore: from the mineral to the magmatic, sedimentary and metamorphic environments, Earth-Sci Rev 161 (2016) 16–129, https://doi.org/10.1016/j.earscirev.2016.07.003.
[11] S.C. Aboudi Mana, M.M. Hanafiah, A.J.K. Chowdhury, Environmental characteristics of clay and clay-based minerals, Geology, ecology, and landscapes. 1 (2017) 155–161, https://doi.org/10.1080/24749508.2017.1361128.
[12] J.S. Moya, B. Cabal, S. Lopez-Esteban, J.F. Bartolomé, J. Sanz, Significance of the formation of pentahedral aluminum in the reactivity of calcined kaolin/metakaolin and its applications, Ceram. Int. 50 (2024) 1329–1340, https://doi.org/10.1016/j.ceramint.2023.10.304.
[13] H. Wang, C. Li, Z. Peng, S. Zhang, Characterization and thermal behavior of kaolin, J. Therm. Anal. Calorim. 105 (2011) 157–160, https://doi.org/10.1007/s10973-011-1385-0.
[14] Y. Li, Y. Zhang, Y. Zhang, M. Liu, F. Zhang, L. Wang, Thermal behavior analysis of halloysite selected from Inner Mongolia Autonomous Region in China, J. Therm. Anal. Calorim. 129 (2017) 1333–1339, https://doi.org/10.1007/s10973-017-6324-2.
[15] A. Zhang, L. Kang, Y. Zhang, D. Ding, Y. Zhang, Thermal behaviors and kinetic analysis of two natural kaolinite samples selected from Qingshuihe region in Inner Mongolia in China, J. Therm. Anal. Calorim. 145 (2021) 3281–3291, https://doi.org/10.1007/s10973-020-09869-4.
[16] P. Alfonso, L.A. Penedo, M. García-Vallès, S. Martínez, A. Martínez, J.E. Trujillo, Thermal behaviour of kaolinitic raw materials from San José (Oruro, Bolivia), J. Therm. Anal. Calorim. 147 (2022) 5413–5421, https://doi.org/10.1007/s10973-022-11245-3.
[17] G.W. Brindley, M. Nakahira, Kinetics of dehydroxylation of kaolinite and halloysite, J. Am. Ceram. Soc. 40 (1957) 346–350, https://doi.org/10.1111/j.1151-2916.1957.tb12549.x.
[18] A.K. Chakraborty, D.K. Ghosh, Reexamination of the kaolinite-to-mullite reaction series, J. Am. Ceram. Soc. 61 (1978) 170–173, https://doi.org/10.1111/j.1151-2916.1978.tb09264.x.
[19] J.S. Moya, M.I. Osendi, Microstructure and mechanical properties of mullite/ZrO_2 composites, J. Mater. Sci. 19 (1984) 909–2914, https://doi.org/10.1007/BF01026966.
[20] J.S. Moya, C.J. Serna, J.E. Iglesias, On the formation of mullite from kandites, J. Mater. Sci. 20 (1985) 32–36, https://doi.org/10.1007/BF00555895.
[21] A.K. Chakraborty, DTA study of preheated kaolinite in the mullite formation region, Thermochim. Acta 398 (2003) 203–209, https://doi.org/10.1016/S0040-6031(02)00367-2.

[22] W. Chen, J.T. Li, Z. Wang, W.A. Algozeeb, D.X. Luong, C. Kittrell, J.M. Tour, Ultrafast and controllable phase evolution by flash joule heating, ACS. Nano 15 (2021) 11158–11167, https://doi.org/10.1021/acsnano.1c03536.
[23] P. Huang, R. Zhu, X. Zhang, W. Zhang, Effect of free radicals and electric field on preparation of coal pitch-derived graphene using ultrafast Joule heating, Chem. Eng. J. 450 (2022) 137999, https://doi.org/10.1016/j.cej.2022.137999.
[24] C. Wang, W. Ping, Q. Bai, H. Cui, R. Hensleigh, R. Wang, L. Hu, A general method to synthesize and sinter bulk ceramics in seconds, Science (1979) 368 (2020) 521–526, https://doi.org/10.1126/science.aaz7681.
[25] Y. Wang, Y. Zhang, Q. Zhou, Y. Zhang, J. Sun, Thermal kinetics analysis of coal-gangue selected from Inner Mongolia in China, J. Therm. Anal. Calorim. 131 (2018) 1835–1843, https://doi.org/10.1007/s10973-017-6642-4.
[26] H. Cheng, J. Yang, Q. Liu, J. He, R.L. Frost, Thermogravimetric analysis-mass spectrometry (tg-ms) of selected chinese kaolinites, Thermochim. Acta 507 (2010) 106–114, https://doi.org/10.1016/j.tca.2010.05.007.
[27] J.C.F. Segura, V.E.R. Cruz, J.J.P. Bueno, E.M.L. Ascencio, F.L. García, Characterization and electrochemical treatment of a kaolin, Appl. Clay. Sci. 146 (2017) 264–269, https://doi.org/10.1016/j.clay.2017.06.004.
[28] A. Basu, M. Mookherjee, S. Clapp, S. Chariton, V.B. Prakapenka, High-pressure Raman scattering and X-ray diffraction study of kaolinite, $Al_2Si_2O_5$ (OH)4, Appl. Clay. Sci. 245 (2023) 107144, https://doi.org/10.1016/j.clay.2023.107144.
[29] N. Ranjbar, C. Kuenzel, J. Spangenberg, M. Mehrali, Hardening evolution of geopolymers from setting to equilibrium: a review, Cement Concr. Compos. 114 (2020) 103729, https://doi.org/10.1016/j.cemconcomp.2020.103729.
[30] H. Cheng, Q. Liu, X. Cui, Q. Zhang, Z. Zhang, R.L. Frost, Mechanism of dehydroxylation temperature decrease and high temperature phase transition of coal-bearing strata kaolinite intercalated by potassium acetate, J. Colloid. Interface Sci. 376 (2012) 47–56, https://doi.org/10.1016/j.jcis.2012.02.065.
[31] W.F. Moll, Baseline studies of the clay minerals society source clays: geological origin, Clays. Clay. Miner. 49 (2001) 74–380, https://doi.org/10.1346/CCMN.2001.0490503.
[32] W. Ge, H. Mao, J. Chen, F. Min, H. Liu, S. Song, Understanding the thermal activation behavior of montmorillonite and kaolinite at atomic level by ReaxFF molecular dynamics simulations, Appl. Clay. Sci. 251 (2024) 107313, https://doi.org/10.1016/j.clay.2024.107313.